Journal of Nano- and Electronic Physics
Vol. **18** No 5, 05034(7pp) (2026)

Журнал нано- та електронної фізики
Том **18** № 5, 05034(7cc) (2026)

OPEN ACCESS

REGULAR ARTICLE

EBG-Integrated Quad-Band Decagonal Slitted Microstrip Patch Antenna for 5G Wireless Systems

Faez M. B. Abdo[1,*], Abdul Guddoos S. A. Gaid[1,†], Mukhtar Ghaleb[2], Mohammad Ahmed Alomari[3], Imran Mohd Ibrahim[3]

[1] *Faculty of Engineering & Information Technology, Taiz University, Taiz, Yemen*
[2] *Department of Information Systems and Cybersecurity, College of Computing and Information Technology, University of Bisha, 67714 Bisha, Saudi Arabia*
[3] *Faculty of Artificial Intelligence and Cyber Security (FAIX), Universiti Teknikal Malaysia Melaka (UTeM), Melaka, Malaysia*
[4] *Centre for Telecommunication Research and Innovation (CeTRI), Fakulti Teknologi Kejuruteraan Elektronik dan Komputer, Universiti Teknikal Malaysia Melaka (UTeM), Melaka, Malaysia*

(Received 27 April 2026; revised manuscript received 20 October 2026; published online 28 October 2026)

With the rapid advancement of 5G wireless networks, there is a growing need for compact, high-performance antennas capable of operating across multiple mm-Wave bands. Microstrip patch antennas are ideal for 5G applications due to their low profile and ease of integration. However, achieving high gain, wide bandwidth, and high radiation efficiency in compact forms with multiband functionality antennas remains challenging. This paper presents a decagonal quad-band microstrip antenna integrated with mushroom-type Electromagnetic Band Gap (EBG) structures, designed for operation at 28, 38, 45, and 60 GHz. The single-element antenna, fabricated on a 12 × 12 × 0.66 mm^3 Arlon AD 255C substrate, incorporates three slits and ten mushroom-type EBG cells to enhance impedance matching and radiation performance. Simulated results show bandwidths of 1.7 GHz, 2.5 GHz, 5 GHz, and 15 GHz with peak gains of 6.5 dBi, 9 dBi, 8.9 dBi, and 8 dBi at the resonant frequencies, respectively. The proposed design also achieves efficiencies ranging from 78 % to 93.5 %. The proposed antenna offers compact size, high gain, and quad-band operation, making it a strong candidate for integration into next-generation 5G mobile devices.

Keywords: Quad-band, Slitted microstrip antenna, EBG-integrated antenna, Wireless systems, 5G.

DOI: 10.21272/jnep.18(5).05034 PACS number: 84.40.Ba

1. INTRODUCTION

5G wireless networks achieve their promised high data rates and ultra-low latencies through operating across two primary spectrum ranges; that's the sub-6 GHz and millimeter-wave (mm-Wave) bands. While the sub-6 GHz spectrum is highly congested due to numerous wireless systems, the mm-Wave spectrum offers significantly wider bandwidths, enabling higher throughput and lower latency. Regulatory bodies such as the ITU and the FCC have designated several critical mm-Wave ranges, specifically highlighting the 28, 38, 60, and 73 GHz bands as essential for future network deployment [1]. Among these, the 28, 38, and 60 GHz bands are particularly advantageous for high-speed mobile access, though they must overcome significant propagation challenges, including high path loss, atmospheric absorption, and signal attenuation [2].

To mitigate these channel impairments, high-gain antenna solutions are vital. While aperture antennas provide the necessary directivity, their bulky nature makes them difficult to integrate into modern hardware, spurring the development of microstrip patch antennas as a compact and cost-effective alternative [1]. However, because single-element patch antennas typically yield low gain (below 5 dBi), researchers employ specialized enhancement techniques such as utilizing slots, Electromagnetic Band Gap (EBG) structures, and multi-element arrays [2]. Moreover, the demand for compact multiband antennas is increasing, as modern devices demand operation across multiple frequency bands. A single integrated multiband antenna can replace several individual antennas, thereby reducing space requirements and improving system efficiency [3].

Numerous multiband antenna designs emerged for 5G applications. Tiwari et al. [4] introduced a rectangular patch antenna featuring two circular slots (12 × 3 mm^2) on a Rogers 3003 substrate, which operated at 28/38 GHz with gains of 6.11/7.15 dBi and 1.54 GHz bandwidth. In [5], the authors proposed a rectangular microstrip patch with slots and an inset feed on a Rogers RT/Duroid 5880 with dimensions of 33 × 27 mm^2. This antenna achieved gains of 7.82 and 8.98 dBi, with bandwidths of 1.1 GHz and 1.3 GHz at 28 GHz and 38 GHz, respectively. El-Hakim and Mohamed [6] introduced a design that integrated two rectangular and circular

* Correspondence e-mail: faeez.abdo.std@taiz.edu.ye
† quddoos.gaid@taiz.edu.ye

© 2026 The Author(s). Journal of Nano- and Electronic Physics published by Sumy State University. This article is distributed under the terms and conditions of the Creative Commons Attribution (CC BY) license.

Cite this article as: Faez M. B. Abdo, et al., *J. Nano- Electron. Phys.* 18 No 5, 05034 (2026) https://doi.org/10.21272/jnep.18(5).05034

patches within a single square patch on Rogers RT/Duroid 4003 (24 × 24 mm²). Their design yielded gains of 9.75 and 10.75 dBi and bandwidths of 7 GHz and 20 GHz at 28 and 60 GHz, respectively. A compact monopole rectangular patch incorporating a circular slot, elliptical patch, and a defective ground structure (DGS) on RT/Duroid 5880 (4.4 × 5 mm²) was introduced in [7], supporting 28/38/60 GHz operation with 2-5 dBi gain and 48.3 GHz bandwidth. In [8], an octagonal radiator with microstrip feeding on Rogers 5880 (14 × 16 mm²) achieved gains ranging from 1 to 15 dBi and an ultra-wide bandwidth of 334.17 GHz (3.71-337.88 GHz). A triple-integrated elliptical patch with a tapered feed line and DGS on Rogers RT/Duroid (27 × 29.5 mm²) was reported in [9], offering 2-8.15 dBi gain and 41.59 GHz bandwidth across 1.91-43.5 GHz. In [10], the authors proposed a rectangular patch antenna on a 10.2 × 8.2 mm² FR4 epoxy, optimized using a binary-coded genetic algorithm. This design achieved gains of 7.7, 12.1, and 8.2 dBi at 28, 40, and 47 GHz, with a 3.1 GHz bandwidth. In addition, the authors in [11] presented a rectangular patch antenna incorporating C- and U-shaped slots with a coplanar waveguide (CPW) feed. This antenna, fabricated on Rogers RT/Duroid 5880 with compact dimensions of 4 × 3 mm², achieved gains of 5.29, 7.49, and 9 dBi at 28, 38, and 60 GHz, respectively. It also offered a total bandwidth of 17.5 GHz and an average S11 of – 22 dB. Furthermore, several studies [12-18] have proposed multiband antennas. However, most of these designs operate in two or three bands, with modest gains that are typically inadequate to compensate for the substantial path losses at mm-Wave frequencies. Conversely, some works [19] have achieved high gains and wide bandwidths but lack multiband functionality.

Despite the significant progress, balancing high gain, compactness, and simplicity remains a major challenge. However, developing a high-gain, quad-band single-element antenna that rivals the performance of arrays remains an open research problem. This study presents a compact single-element microstrip antenna with quad-band operation and high performance. The single-element design features a decagonal patch with three rectangular slits and ten embedded EBG cells. The main contributions of this work are as follows:

1. **Quad-band operation:** The proposed patch antenna covers four key mm-Wave bands: 28, 38, 45, and 60 GHz. This design employs three rectangular slits and ten mushroom-type EBG cells (five per side) into the radiating patch. The design has improved return loss, gain, and radiation efficiency, making it suitable for 5G use.
2. **Compact form factor:** The single-element antenna is compact, making it ideal for integration into space-limited 5G mobile devices.

The remainder of this paper is as follows: **Section 2** presents the antenna design methodology, while **Section 3** discusses the simulation results and performance evaluation. **Section 4** offers a comparative analysis with related literature, and finally, **Section 5** concludes with final remarks and suggestions for future work.

2. THE ANTENNA DEVELOPMENT

2.1 Basic Antenna Development

This subsection outlines the design and optimization of a quad-band EBG-integrated microstrip patch antenna, intended for 5G wireless systems. Fig. 1 depicts the basic antenna reported in [3], which is used to develop the EBG-integrated antenna targeting four specific frequency bands: 28 GHz, 38 GHz, 45 GHz, and 60 GHz.

The design employs an Arlon AD 255C substrate with a dielectric constant (εr) of 2.6, a loss tangent (tan δ) of 0.0014, and a thickness of 0.66 mm. The radiating patch on the upper side and the ground plane on the bottom side of the substrate comprise copper sheets with a thickness of 0.035 mm. A stepwise design approach, using CST simulation software, was adopted to optimize the antenna. The goal of this stepwise iterative method is to tune the antenna to its four resonant modes and adjust the resonant frequencies at the intended bands.

The optimized basic antenna, shown in Fig. 1, is compact, measuring 12 × 12 × 0.66 mm³. A microstrip line with length (lf = 2.5 mm) and width (wf = 0.6 mm) feeds the antenna. The radiating patch features a decagonal geometry with a radius of rp = 3.7 mm and three rectangular slits with optimized dimensions summarized in Table 1.

2.2 Enhancing Antenna Performance Using EBG

EBG structures play a vital role in improving the performance of microstrip antennas by effectively suppressing surface wave propagation. These surface waves often trap energy and hence, reduce both radiation efficiency and gain. By blocking these unwanted modes, EBGs help redirect otherwise lost energy into a useful radiation. Moreover, their in-phase reflection characteristics promote constructive interference with the antenna's radiated signals, enhancing forward directivity and focusing the emitted energy. As a result, EBGs contribute to significant improvements in antenna return loss, radiation efficiency, gain, and overall functionality, making them an essential technology for advanced wireless systems such as 5G.

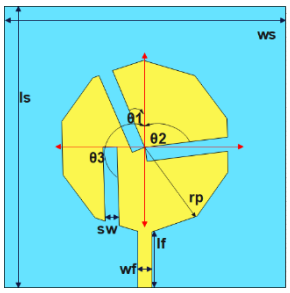
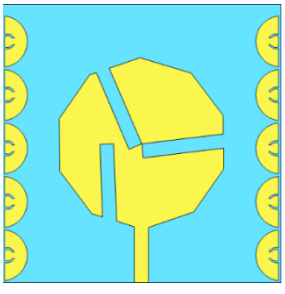
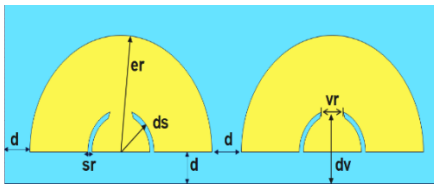


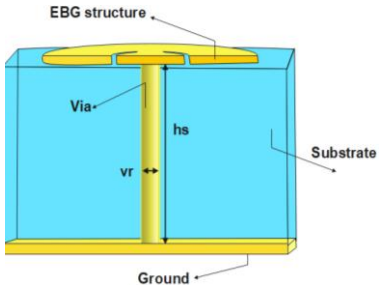
Fig. 1 – Geometry of the basic optimized antenna



(a)



(b)



(c)

Fig. 2 – The proposed EBG-integrated antenna: (a) final optimized design, (b) upper view of the EBG unit cell, (c) side view of the EBG unit cell

Table 1 – The slits' dimensions of the optimized basic patch antenna

Slit 1			
$\theta 1$ (deg)	sw (mm)	sl (mm)	
		Right-side	Left-side
23	0.6	3.53	3.58
Slit 2			
$\theta 2$ (deg)	sw (mm)	sl (mm)	
		Upper-side	Lower-side
-83	0.6	3.55	3.47
Slit 3			
$\theta 3$ (deg)	sw (mm)	sl (mm)	
		Right-side	Left-side
182	0.6	3.35	3.13

As illustrated in Fig. 2(a), ten mushroom-type semicircular EBG cells were symmetrically integrated with the antenna, five cells positioned on each side of the radiating patch. These EBG cells, shown in Fig. 2(b) and (c), employ vias to connect to the ground plane. Table 2 summarizes optimized dimensions of EBG cells. The inclusion of EBG structures introduces a bandgap filtering effect that aligns with the antenna's operational frequency bands, as demonstrated in Fig. 3, thereby significantly enhancing overall performance.

Consequently, slight shifts in the resonant frequencies occur at 28 GHz, 37.9 GHz, 44.8 GHz, and 61.4 GHz. These frequencies exhibited significantly improved reflection coefficients of – 15.7 dB, – 28.4 dB, – 33.6 dB, and – 58.5 dB, respectively. Additionally, the corresponding impedance bandwidths were measured as follows: 1.7 GHz for the 28 GHz band (spanning 27.2-28.9 GHz), 2.5 GHz for the 37.9 GHz band (ranging from 37-39.5 GHz), 5 GHz for the 44.8 GHz band (41.5-46.5 GHz), and 15 GHz for the 61.4 GHz band (extending from 52.8-67.8 GHz), as illustrated in Fig. 4.

EBG structures also improved gains in the four operational bands to 6.5 dBi, 9 dBi, 8.9 dBi, and 9 dBi, respectively, with significantly improved radiation efficiencies. There is a peak gain improvement by 1.8 dBi, where the gain was 8.7 dBi at 55 GHz, and the EBG structures improved it to 10.5 dBi, as shown in Fig. 5. Radiation efficiency peaked at 93.5 % at 41.7 GHz and was lowest at 78 % at 28 GHz, as shown in Fig. 6.

Table 3 summarizes the antenna performance in terms of resonance frequencies, bandwidth, return loss, radiation efficiency, and gain before and after integration of the EBG unit cells.

Table 2 – The optimized dimensions of EBG cells

Param	***d***	***dv***	***ds***	***er***	***sr***	***vr***	***hs***
Value (mm)	0.1	0.375	0.4	1.1	0.05	0.3	0.66

Table 3 – Performance comparison between the basic and the EBG-integrated antennas

Param	**Basic Ant**				**EBG-Integrated Ant**			
f_r **(GHz)**	28	37.8	44.8	61.3	28	37.9	44.8	61.4
S_{11} **(dB)**	– 14.7	– 23.8	– 20.7	– 26.3	– 15.7	– 28.4	– 33.6	– 58.5
BW (GHz)	1.6	2.5	5	15	1.7	2.5	5	15
Gain (dBi)	5.9	7.8	7.5	7.4	6.5	9	8.9	8
Rad. Eff. (%)	86	88	92	82	78	91	92	84

3. SIMULATION RESULTS AND DISCUSSION

This work utilizes CST Studio Suite to design and optimize the proposed antenna. Comparative simulations using Ansys HFSS ensure the reliability of the results and reinforce confidence in the final design.

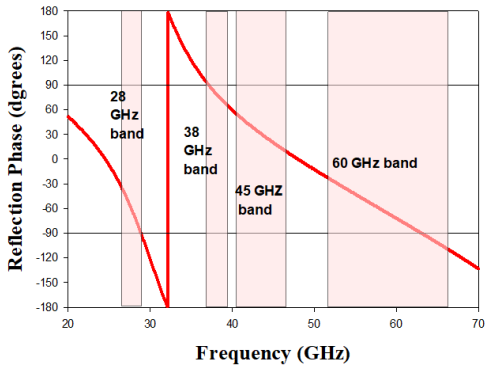


Fig. 3 – Reflection phase of the EBG structure

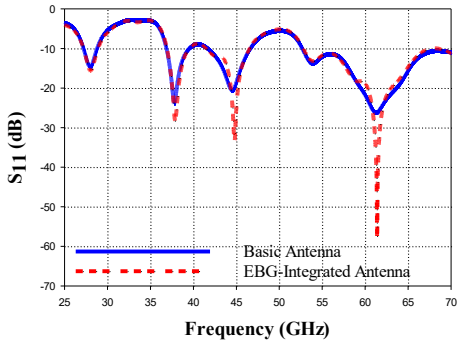


Fig. 4 – Simulated S_{11} performance of the basic and the EBG-integrated antennas

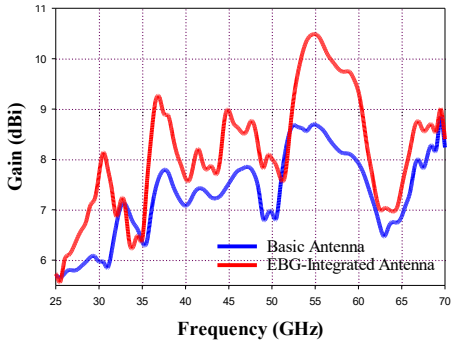


Fig. 5 – Simulated gain performance of the basic and EBG-integrated antennas

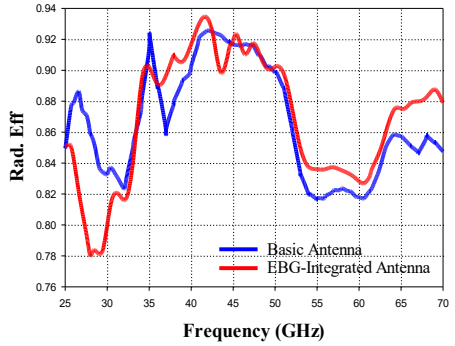


Fig. 6 – Simulated radiation efficiency of the basic and EBG-integrated antennas

The excellent correlation between CST and HFSS-based results not only confirms the robustness of the antenna design but also minimizes the likelihood of discrepancies during fabrication. This dual-platform simulation strategy facilitates a comprehensive and rigorous evaluation of the antenna's behavior across its entire operational bandwidth. Accordingly, a comparison of key performance metrics obtained from both CST and HFSS demonstrates a high degree of consistency and accuracy.

a) S_{11} Parameter Behavior

Fig. 7 presents S_{11} characteristics of the proposed antenna, derived from CST and HFSS simulations. The CST simulation reveals four distinct resonant frequencies at 28 GHz, 37.9 GHz, 44.8 GHz, and 61.4 GHz, corresponding to reflection coefficients of – 15.7 dB, – 28.4 dB, – 33.6 dB, and – 58.5 dB, respectively. These resonances are associated with bandwidths of 1.7 GHz, 2.5 GHz, 5 GHz, and 15 GHz.

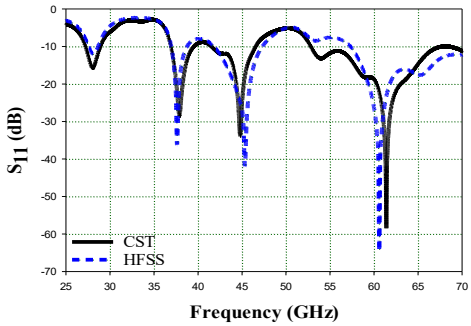


Fig. 7 – S_{11} performance of the proposed antenna using CST and HFSS

Similarly, the HFSS simulation yields closely aligned resonant frequencies at 28.1 GHz, 37.6 GHz, 45.3 GHz, and 60.6 GHz, with corresponding reflection coefficients of – 12.1 dB, – 35.9 dB, – 41.6 dB, and – 60.6 dB. The respective bandwidths observed in HFSS are 1.1 GHz, 1.7 GHz, 5.5 GHz, and 12.6 GHz.

Overall, the results from both electromagnetic solvers exhibit strong correlation, with only minor deviations. These discrepancies are well within acceptable limits and primarily attributed to differences in simulation methodologies, such as meshing strategies and numerical solvers inherent to each platform.

b) Voltage Standing Wave Ratio (VSWR)

Fig. 8 presents VSWR characteristics obtained from CST and HFSS simulations. The CST simulation yields VSWR values of 1.393, 1.079, 1.043, and 1.002 at resonant frequencies of 28, 37.9, 44.8, and 61.4 GHz, respectively. In comparison, the HFSS simulation produces slightly shifted resonant frequencies with corresponding VSWR values of 1.662, 1.054, 1.075, and 1.002. Both results demonstrate excellent impedance matching, as indicated by low VSWR values and minimal signal reflection across all operational bands. Furthermore, the impedance bandwidths satisfying the VSWR ≤ 2 criterion align closely with those derived from the S_{11} curves for values ≤ – 10 dB. This strong correlation between the two simulation platforms further validates the accuracy of the design process and confirms the reliability of the simulation results.

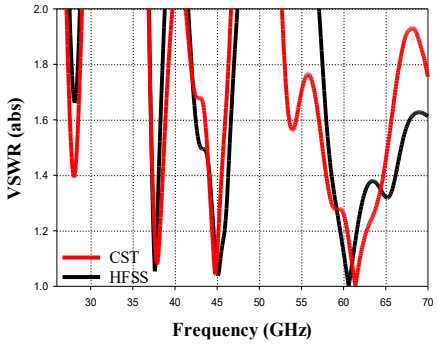


Fig. 8 – VSWR performance of the proposed antenna using CST and HFSS

c) Far-Field Radiation Characteristics

Fig. 9 presents the antenna's 2D radiation patterns obtained from CST and HFSS simulations. In both cases, the antenna exhibits a directional radiation pattern in the far-field region. CST simulation results show peak gains of 6.5/9/8.9/8 dBi at the respective resonant frequencies. Similarly, the HFSS simulation confirms a directional radiation profile with gains of 7.7/10.2/8.5/7.7 dBi. Despite slight differences, both simulation tools reveal consistent radiation behavior, supporting the reliability of the design.

Fig. 10 illustrates the antenna's gain performance across its operational frequency bands. In CST simulations, the gain varies from a minimum of 6.4 dBi at 27.5 GHz to a maximum of 10.5 dBi at 55 GHz. In comparison, the HFSS results show a gain range from 7.2 dBi at 27.6 GHz to a peak value of 10.4 dBi at

66.7 GHz. Overall, the gain trends and radiation characteristics obtained from CST and HFSS are in acceptable agreement. These results further validate the antenna's consistent performance and the effectiveness of the design approach.

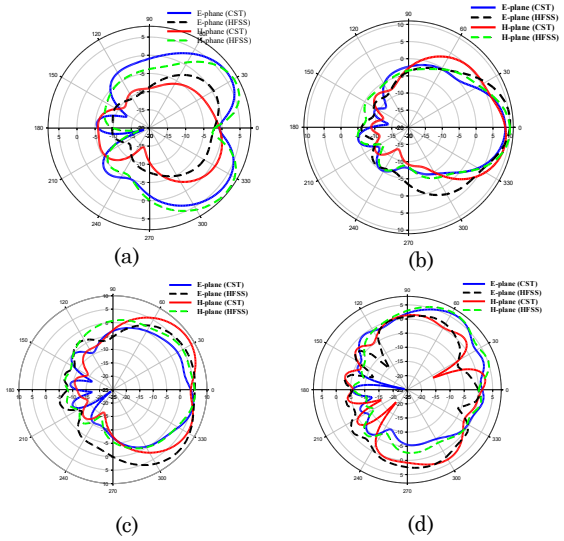


Fig. 9 – 2D radiation patterns of the proposed antenna using CST and HFSS at: (a) 28 GHz, (b). 37.9 GHz, (c). 44.8 GHz, and (d). 61.4 GHz.

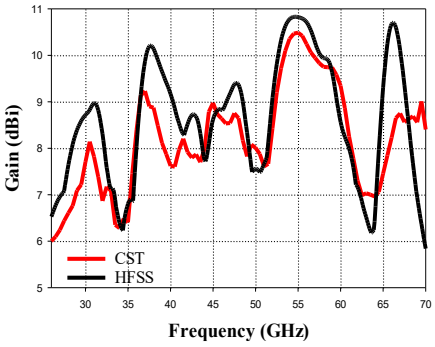


Fig. 10 – Gain performance of the proposed antenna using CST and HFSS

d) Surface Current Distribution

Fig. 11 illustrates the surface current distributions at the antenna's resonant frequencies, 28/37.9/44.8/61.4 GHz. At 28 GHz, the currents are strongly concentrated along the feed line and circulate coherently around the radiator perimeter, indicating the fundamental mode with efficient edge radiation. At 37.9 and 44.8 GHz, the current splits into multiple lobes and localizes at the edges of the slits. A pronounced current accumulation also appears along the curved slits of the EBG cells, highlighting their role in suppressing surface-wave propagation and redirecting electromagnetic energy into free space. At 61.4 GHz, the currents become more compact and confined to fine features near the feed, consistent with a high-order collective mode at mm-wave frequencies. Across all bands, the EBG surroundings confine energy to the radiator, mitigate ground-wave leakage, and stabilize the input match – accounting for the observed improvements in realized gain and radiation efficiency.

4. COMPARISON WITH RELATED WORKS

Table 4 provides a comparative analysis of multiband microstrip antennas designed for the frequency range 20 to 90 GHz. This table consolidates data from recent studies, offering a comprehensive overview of key parameters including antenna size, frequency bands, S_{11}, bandwidth, gain, and radiation efficiency.

Table 4 – The comparison details of the presented antenna with recent published works

Ref	Ant. size (mm^2)	f (GHz)	BW (GHz)	Gain (dBi)	Rad. Eff. (%)
[4]	12 × 3	28/38	0.68/0.86 (1.54)	6.1/7.2	70/80
[5]	33 × 27	28/38	1.1/1.3 (2.4)	7.82/8.98	96/95.5
[6]	24 × 24	28/60	7/20 (27)	9.75/10.75	85/84
[7]	4.4 × 5	28/38/60	21.7 to 70 (48.3)	2 to 5	90
This work	12 × 12	28/38/45 /60	1.7/2.5/5/ 15 (24.2)	6.5/9/8.9/9	78-93.5

Regarding antenna size, the proposed single-element design measures 12 × 12 mm^2, which is larger than certain antennas reported in [4] and [7]. Nevertheless, it outperforms these designs in radiation efficiency and gain and provides a wider bandwidth than the design reported in [4]. The proposed antenna also has a smaller form than antennas described in [5] and [6].

In summary, the proposed antenna is quad-band, achieving an exceptional balance of low return loss, high gain, and radiation efficiency, thereby demonstrating superior performance relative to existing designs in the literature. This success not only validates the effectiveness of the adopted design methodology but also underscores promising avenues for further advancements in multiband antenna technologies.

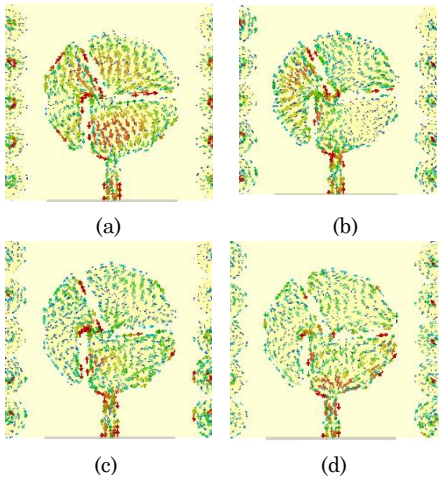


Fig. 11 – Surface current distribution of the proposed EBG-integrated antenna: (a) 28 GHz, (b) 37.9 GHz, (c) 44.8 GHz, and (d) 61.4 GHz

5. CONCLUSION

This study introduced an EBG-integrated decagonal quad-band antenna. The proposed antenna operates within the 28, 38, 45, and 60 GHz frequency bands. The design and optimization processes employed CST Studio Suite, while results validation used Ansys HFSS, ensuring greater accuracy and precision. The proposed element achieves wide bandwidths across the four bands, specifically 1.7 GHz (27.2 to 28.9 GHz), 2.5 GHz (37 to 39.5 GHz), 5 GHz (41.5 to 46.5 GHz), and 15 GHz (52.8 to 67.8 GHz). The element exhibits gains of 6.5, 9, 8.9, and 8 dBi at the respective resonant frequencies of 28, 37.9, 44.8, and 61.4 GHz. Additionally, the radiation efficiency ranges from 78 % to 93.5 %, demonstrating effective power utilization. Due to the lack of necessary facilities, future efforts will focus on fabricating and measuring the design, and extending it to a MIMO antenna configuration, alongside an investigation of its Specific Absorption Rate (SAR) characteristics.

ACKNOWLEDGMENT

The authors would like to express their sincere gratitude to the Deanship of Graduate Studies and Scientific Research at the University of Bisha for supporting this work through the Fast-Track Research Support Program. The authors also gratefully acknowledge the Centre for Research and Innovation Management (CRIM), Universiti Teknikal Malaysia Melaka (UTeM), for their valuable support and assistance throughout this research.

REFERENCES

1. A.E. Farahat, K.F. Hussein, *Sensors* **26** No 6, 1890 (2026) https://doi.org/10.3390/s26061890.
2. M. Sharma, B.R. Perli, G. Singla, T. Addepalli, S. Medasani, B.S. Sridevi, T. Ali, *PloS ONE* **21** No 2, e0342022 (2026) https://doi.org/10.1371/journal.pone.0342022.
3. F.M.B. Abdo, A.G.S. Gaid, M.A. Alomari, I.M. Ibrahim, M. Ghaleb, *J. Nano- Electron. Phys.* **18** No 1, 01033 (2026) https://doi.org/10.21272/jnep.18(1).01033.
4. R.N. Tiwari, O.S. Sai, D. Sharma, M.S. Kumar, P. Singh, P. Kumar, S. Rajasekaran, *Res. Eng.* **24**, 103212 (2024) https://doi.org/10.1016/j.rineng.2024.103212.
5. B.O. Icmez, C. Kurnaz, *Appl. Sci.* **15** No 7, 3993 (2025) https://doi.org/10.3390/app15073993.
6. H. El-Hakim, H.A. Mohamed, *J. Infrared Millim. Terahertz Waves* **44** No 9, 752 (2023) https://doi.org/10.1007/s10762-023-00937-y.
7. V. Sharma, N.K. Mishra, A. Agarwal, N.L. Gupta, *Gazi Univ. J. Sci.* **37** No 1, 211 (2024) https://doi.org/10.35378/gujs.1178594.
8. N. Suguna, S. Revathi, *Appl. Sci.* **13** No 8, 5057 (2023) https://doi.org/10.3390/app13085057.
9. M. Ayyappan, P. Patel, *IEEE Access* **10**, 76031 (2022) https://doi.org/10.1109/ACCESS.2022.3185241.
10. Dejen, J. Jayasinghe, M. Ridwan, J. Anguera, *AIMS Electron. Electr. Eng.* **6** No 1, 1 (2022) https://doi.org/10.3934/electreng.2022001.
11. S. Ahmad, H. Boubakar, S. Naseer, M.E. Alim, Y.A. Sheikh, A. Ghaffar, N.O. Parchin, *Sensors* **22** No 20, 8012 (2022) https://doi.org/10.3390/s22208012.
12. O.Y. Saeed, A.A. Saeed, A.S. Gaid, A.M. Aoun, A.A. Sallam, *2021 International Conference of Technology, Science and Administration (ICTSA)*, **1** (IEEE: 2021) https://doi.org/10.1109/ICTSA52017.2021.9406521.
13. A.S. Gaid, A.M. Alhakimi, O.Y. Sae'ed, M.S. Alasadee, A.A. Ali, *International Conference of Reliable Information and Communication Technology*, 663 (Cham: Springer International Publishing: 2019) https://doi.org/10.1007/978-3-030-33582-3_62.
14. A.S. Gaid, M.A. Ali, *Iraqi J. Electr. Electron. Eng.* **19** No 2, 179 (2023) https://doi.org/10.37917/ijeee.19.2.20.
15. F.M.B. Abdo, A.S. Gaid, M.M. Saeed, R.A. Saeed, M.A. Alomari, *2025 5th International Conference on Emerging Smart Technologies and Applications (eSmarTA)*, 1 (IEEE: 2025) https://doi.org/10.1109/eSmarTA66764.2025.11132136.
16. A.S. Gaid, A.A. Sallam, A.M. Aoun, A.A. Saeed, O.Y. Saeed, *International Conference of Reliable Information and Communication Technology*, 728 (Cham: Springer International Publishing: 2020) https://doi.org/10.1007/978-3-030-70713-2_66.
17. A.S. Gaid, M.H. Qasem, A.A. Sallam, E.Q. Shayea, *International Conference of Reliable Information and Communication Technology*, 717 (Cham: Springer International Publishing: 2020) https://doi.org/10.1007/978-3-030-70713-2_65.
18. A.S. Gaid, O.A. Qaid, M.A. Ameer, F.F. Qaid, B.S. Ahmed, *International Conference of Reliable Information and Communication Technology*, 653 (Cham: Springer International Publishing: 2019) https://doi.org/10.1007/978-3-030-33582-3_61.
19. A.A. Mohammed, A.S. Gaid, M.A. Alomari, Z.A. Shamsan, *J. Radiat. Res. Appl. Sci.* **18** No 4, 101964 (2025) https://doi.org/10.1016/j.jrras.2025.101964.

Інтегрована з EBG-структурою чотирисмугова десятикутна мікросмужкова антена зі щілинами для бездротових систем 5G

Faez M. B. Abdo[1], Abdul Guddoos S. A. Gaid[1], Mukhtar Ghaleb[2], Mohammad Ahmed Alomari[3], Imran Mohd Ibrahim[3]

[1] *Faculty of Engineering & Information Technology, Taiz University, Taiz, Yemen*
[2] *Department of Information Systems and Cybersecurity, College of Computing and Information Technology, University of Bisha, 67714 Bisha, Saudi Arabia*
[3] *Faculty of Artificial Intelligence and Cyber Security (FAIX), Universiti Teknikal Malaysia Melaka (UTeM), Melaka, Malaysia*
[4] *Centre for Telecommunication Research and Innovation (CeTRI), Fakulti Teknologi Kejuruteraan Elektronik dan Komputer, Universiti Teknikal Malaysia Melaka (UTeM), Melaka, Malaysia*

У зв'язку зі стрімким розвитком бездротових мереж 5G зростає потреба в компактних високопродуктивних антенах, здатних працювати в кількох діапазонах міліметрових хвиль (мм-хвиль). Мікросмужкові антени ідеально підходять для систем 5G завдяки своєму низькому профілю та простоті інтеграції. Однак створення компактних багатодіапазонних антен, які б поєднували високий коефіцієнт підсилення, широку смугу пропускання та високий ККД випромінювання, залишається складним завданням. У цій статті представлено десятикутну чотиридіапазонну мікросмужкову антену, інтегровану з електромагнітними забороненими структурами (EBG) «грибоподібного» типу, розроблену для роботи на частотах 28, 38, 45 та 60 ГГц. Ця однолементна антена, виготовлена на підкладці Arlon AD 255C розміром 12 × 12 × 0,66 мм^3, містить три щілини та десять «грибоподібних» EBG-комірок, що дозволяє покращити узгодження імпедансу та характеристики випромінювання. Результати моделювання демонструють смуги пропускання 1,7 ГГц, 2,5 ГГц, 5 ГГц та 15 ГГц із піковими коефіцієнтами підсилення 6,5 дБі, 9 дБі, 8,9 дБі та 8 дБі на відповідних резонансних частотах. Запропонована конструкція також забезпечує ККД у діапазоні від 78 % до 93,5 %. Завдяки компактним розмірам, високому коефіцієнту підсилення та можливості роботи в чотирьох діапазонах, ця антена є перспективним рішенням для інтеграції в мобільні пристрої 5G наступного покоління.

Ключові слова: Чотирисмугова мікросмужкова антена зі щілинами, Антена з інтегрованою структурою EBG, Бездротові системи, 5G.